J Nanopart Res (2020) 22: 40
https://doi.org/10.1007/s11051-020-4757-1

RESEARCH PAPER

Comparison of TiO_2 nanowires and TiO_2 nanoparticles for photodegradation of resorcinol as endocrine model

L. A. Al-Hajji · Adel A. Ismail · M. Alsaidi · S. A. Ahmed · F. Almutawa · A. Bumajdad

Received: 22 November 2019 / Accepted: 13 January 2020 / Published online: 28 January 2020

Abstract In this contribution, comparison of TiO_2 nanowires (TiO_2 NWs) and TiO_2 nanoparticles (TiO_2 NPs) for photodegradation of resorcinol as endocrine model was extensively carried out. The results indicated that X-ray diffraction (XRD) patterns of the TiO_2 NWs exhibited brookite and anatase phases; whereas, the prepared TiO_2 NPs is pure anatase phase. TEM images of TiO_2 NWs exhibit clear nanowire structures with the 2 μm length and diameter of 50–100 nm, while the TiO_2 NPs particle sizes are 5–10 nm. The prepared TiO_2 NWs and TiO_2 NPs were compared with commercial photocatalyst TiO_2-P25 by the determination of their photocatalytic performances. The photocatalytic efficiencies of TiO_2 NWs, TiO_2 NPs, and TiO_2 P25 are amounted to be 98.7%, 98.4%, and 83% within 3-h illumination. However, the photodegradation rates TiO_2 NPs, TiO_2 NWs, and TiO_2-P25 are 12.24×10^{-7} mol L^{-1} min^{-1}, 10.79×10^{-7} mol L^{-1} min^{-1}1, and 5.77×10^{-7} mol L^{-1} min^{-1}, i.e., the photodegradation rates TiO_2 NPs is slightly faster than TiO_2 NWs, and they are significantly greater 2 times than that of commercial photocatalysts TiO_2-P25. The apparent rate constant k (min^{-1}) value of TiO_2 NPs and TiO_2 NWs is higher than that of commercial TiO_2-P25 for 3.3 and 3.25 times, respectively. From the economic point of view, TiO_2 NPs calcined at 400 °C are chosen to be the optimum for saving energy in the preparation step without loss of photocatalytic efficiency.

Keywords TiO_2 nanowires · TiO_2 nanoparticles · Photocatalyst · Photocatalytic efficiency · Endocrine

This article is part of the topical collection: Nanotechnology in Arab Countries

Guest Editor: Sherif El-Eskandarany

L. A. Al-Hajji · A. A. Ismail (✉) · M. Alsaidi · S. A. Ahmed · F. Almutawa
Nanotechnologyand Advanced Materials Program, Energy & Building Research Center, Kuwait Institute for Scientific Research (KISR), P.O. Box 24885, 13109 Safat, Kuwait
e-mail: aaismail@kisr.edu.kw

A. Bumajdad
Chemistry Department, Faculty of Science, Kuwait University, PO Box 5969, 13060 Safat, Kuwait

Introduction

Titanium oxide (TiO_2) exhibits several excellent advantages, such as non-toxicity, long-term stability, environmentally benign nature, and low cost (Varghese et al. 2009; Yu et al. 2013; Yang et al. 2014;

Qiu et al. 2014). In the last three decades, diverse TiO_2 nanomaterials, including nanofibers (Zhu et al. 2011), nanoparticles (Khedr et al. 2019) and nanowires (Lee et al. 2015) have been used for potential photocatalytic applications. However, the TiO_2 shortcomings are the fast recombination of the charge carries and wide band gap, which significantly reduce the photocatalytic performance (Liu et al. 2016; Sang et al. 2014). Controlled shapes of nanostructured materials have received huge attention for both practical applications and fundamental research (Mohamed et al. 2018; Wang et al.

2005; Xia et al. 2009; Ding et al. 2019; Burda et al. 2005). Principally, TiO_2 nanomaterials with one dimensional (1D) like nanorods, nanotubes, and nanowires exhibit considerable importance owing to their large surface area, anisotropic structures, unique physicochemical properties, and quantum confinement effects (Wu et al. 2012; Law et al. 2005; Pan et al. 2001; Xia et al. 2003). Chemical wet processes have been comprehensively carried out to synthesize nanomaterials with comparatively good scalability and low cost (Chen and Mao 2007; Deng et al. 2009). TiO_2 at anatase phase has been employed in various applications including lithium-ion batteries, photocatalysis, and solar cells. It has been reported that the surface property and geometric shape such as TiO_2 NPs and TiO_2 NWs possess superb impact on the TiO_2 physicochemical characteristics (Pan et al. 2011; Sun et al. 2010; Chen et al. 2010). The control of phase structure TiO_2 NWs of anatase to brookite, indicates considerable higher separation charge carriers efficiency due to the synergistic effect (Al-Hajji et al. 2020). Moreover, TiO_2 NWs have higher separation efficiency charge carrier transport through its axial direction. Particularly, the length of the TiO_2 NWs imparts simple recyclability of the photocatalyts after photocatalytic reactions (Deng et al. 2009).

The environmental contamination in factory effluents and water sources of endocrine-disrupting chemicals (EDCs) has revolted considerable attention due to they can generate interference with the endocrine systems functions and hormonal imponderables activity (Huang and Chen 2010). Considerable reverse effects involving sexual underdevelopment, neurobehavioral disorder, birth defects, male and female infertility, varieties of cancers and impaired immune function are encouraged by existence of EDCs. The presence of EDCs is causing some of effects in ecosystem and hence in public health (Brouwers et al. 2011), and thus, an efficient environmental approach for EDC removal from wastewater is highly recommended.

To the best of my knowledge, the comparison between TiO_2 NWs and TiO_2 NPs is not addressed well in the previous published research work related to the photocatalytic oxidation of organic compounds under similar conditions such as photoreactor and light intensity. Therefore, in this contribution, we undertake the direct preparation of TiO_2 NWs and TiO_2 NPs via a facile solvothermal and hydrothermal approach. The prepared TiO_2 NPs and TiO_2 NWs have been compared for photodegradation of resorcinol as endocrine model. Both of the prepared TiO_2 NPs and TiO_2 NWs demonstrate superior photocatalytic performance for the resorcinol photodegradation. The photodegradation rates TiO_2 NPs are slightly faster than TiO_2 NWs, and they are significantly higher 2 times than that of commercial photocatalysts TiO_2-P25.

Experimental

Material

Titanium tetrachloride $TiCl_4$, Ethanol, NaOH, and resorcinol (flakes) 99% were purchased from Sigma-Aldrich and Alpha Chemika. Commercial TiO_2-P25 (20% and 80% of rutile and anatase, respectively) was collected from Evonik Degussa, and used as the photocatalyst and compared with the prepared TiO_2 NPs and TiO_2 NWs.

Preparation of TiO_2 NWs

TiO_2 NWs were synthesized employing the previously published work through hydrothermal process (Zhang et al. 2009). One gram of commercial TiO_2-P25 and 100 mL of 10 M NaOH were mixed and stirred magnetically for 60 min. The produced suspension mixture was placed in a Teflon-lined autoclave and kept in the oven for 48 h at 180 °C. The solid materials were separated after cooling and then were washed few times by 0.1 M HCl to get pH value between 7 and 8 then washed three times by H_2O. The obtained TiO_2 NWs were dried and afterward they were annealed at 800 °C.

Preparation TiO_2 nanoparticles

$TiCl_4$ (7.5 mL) and anhydrous ethanol (120 mL) were magnetically stirred for 30 min. in water bath containing an ice (Elsellami et al. 2018). The obtained white precipitate was put in 150-mL Teflon-lined immersed into the autoclave and then was kept at 150 °C for 24 h. After cooling, the collected TiO2 was separated and then washed three times by water and ethanol. The wet TiO_2 NPs were dried for 6 h at 60 °C and then annealed for 3 h at 400 °C to obtain TiO_2 NPs.

Characterization

JEOL JEM 1230 microscope operating at 120 kV was employed to examine the morphology of TiO_2 NWs and TiO_2 NPs throughout high-resolution transmission electron microscopy (HRTEM). SAP 2010 automatic Micromeritics sorptiometer (USA) was employed to record the N_2 adsorption-desorption isotherms of the TiO_2 NWs and TiO_2 NPs by a computer controlled sorption analyzer. X-ray diffraction (XRD) spectra of the TiO_2 NWs and TiO_2 NPs were measured by a Bruke D8 Advance powder X-ray diffractometer. UV-Vis diffuse reflectance spectra (DRS) were recorded at $\lambda =$ 200–800 nm for TiO_2 NWs and TiO_2 NPs samples using UV-Vis spectrophotometer (UV-2600, Shimadzu), and $BaSO_4$ was employed as a reflectance standard. The bandgap value (*Eg*) was determined by employing the Tauc equation. Photoluminescence (PL) of the prepared samples was performed using xenon lamp at ~ 320 nm with 150-W excitation source throughout spectrofluorophotometer, (RF-6000, Japan, SHIMADZU, 400 W, 50/60 Hz). Bruker Optics IFS66v/s FTIR spectrometer was used to record Raman spectra with FRA-106 Raman attachment.

Photocatalytic tests

The photocatalytic performance was assessed for the photocatalytic degradation of resorcinol (20 ppm) as a model of EDCs over TiO_2 NWs and TiO_2 NPs. Xe-arc lamp (500 W) was employed as the UV light source and it was vertically dived into the photoreactor. 0.5 g of the TiO_2 NWs or TiO_2 NPs was added to 500 mL of resorcinol (20 ppm) which was constantly stirred in dark for 1 h to produce an equilibrium of adsorption/desorption. Oxygen was supplied throughout photocatalytic tests via air pump. Equilibrium of resorcinol adsorption/desorption of onto TiO_2 NWs or TiO_2 NPs was reached after stirring in dark for 1 h. Xe-arc lamp was switched on for 3-h irradiation through photocatalytic system. Resorcinol samples in aqueous solution before and after illumination were taken at certain interval times. The photocatalyst was separated from the solution by filtration via nylon syringe filters (pore size: 0.2 μm for TiO_2 NPs) and (pore size: 0.8 μm for TiO_2 NWs). The separated liquid was analyzed by calculating total organic carbon using multi N/C 3100 Analytik Jena AG, Germany.

Results and discussions

Materials structural

XRD patterns of the synthesized TiO_2 NWs and NPs were presented in Fig. 1. The findings revealed that the synthesized TiO_2 NWs were coincided with the XRD data standard of anatase (JCPDS No. 21-1272) and brookite (PDF no. 39-1360) phases. XRD of the TiO_2 NPs was displayed in Fig. 1, curve a. The findings indicated that the peaks were assigned at $2\theta = 25.40°$ (101), 37.96° (004), 48.19° (200), 54.06° (105), and 55.30° (211) (Li and Zeng 2011), which corresponded to pure anatase phase. The synthesized TiO_2 NWs

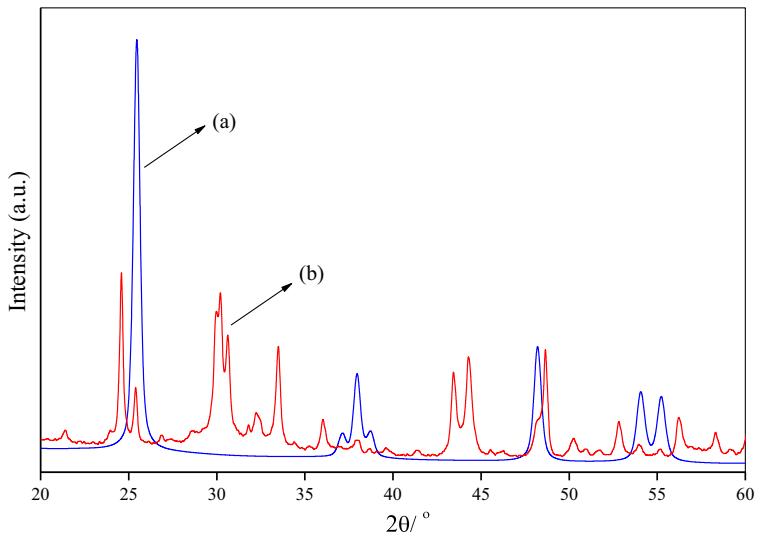

Fig. 1 XRD patterns for TiO_2 NPs calcined at 400 °C (**a**) and TiO_2 NWs calcined at 800 °C (**b**)

which show various contents of anatase and brookite, owing to the peaks of anatase and brookite, have been overlapped (Fig. 1, curve b). The peak characteristic (121) was assigned at $2\theta = 30.81°$, which it was obviously confirmed the brookite phase (Fig. 1, curve b). The main peak (101) of the anatase phase was located at $2\theta = 25.28°$, which it overlaps the TiO_2 brookite phase at $2\theta = 25.35°$ and 25° with (111) and (120), respectively. The average crystallite sizes (D) is roughly determined by Scherrer equation (Hu et al. 2011):

$D = K\lambda / (\beta \cos\theta)$.

where K is the Scherrer constant (0.89), θ is the diffraction angle and β is the half-peak width and λ is the wavelength of the X-ray (1.54 A). The calculated crystallite sizes of the TiO_2NPs and TiO_2 NWs are amounted to be 19.88 and 43.21 nm, respectively. The crystallinity of the TiO_2NPs and TiO_2 NWs was additionally emphasized by Raman spectroscopy (Fig. 2). The findings of TiO_2 NPs revealed that the features anatase peaks at 144, 196.95, 394.9, 514.51, and 637.38 cm^{-1} were assigned without any impurities, which is in consistent with XRD. However, Raman spectrum of TiO_2 NWs exhibited that anatase and brookite phases were obviously assigned (Fig. 2). There are 8 Raman brookite peaks located at A1g (136, 158, 196, 222, 412, and 661 cm^{-1}), B1g (275 cm^{-1}), and B2g (478 cm^{-1}) (Li et al. 2014). In addition, there are four Raman-active modes of the anatase phase with Eg, B1g, B1g, and Eg symmetries which were located at 197, 410, 677, and 871 cm^{-1} (Li et al. 2014). In general, the formation phase of TiO_2 NPs is anatase; however, the synthesized TiO_2 NPs phase is mixture of anatase and brookite.

N_2 adsorption-desorption isotherm was conducted to locate the pore structures of the TiO_2 NPs and TiO_2 NWs (Fig. 3). The results indicated that TiO_2 NPs exhibited a typical type of IV hysteresis, indicating narrow pore size distribution and microporosity (Sing et al. 1985). In addition, the TiO_2 NWs hysteresis loops type is H3, implying the existence of slit-like pores (Fig. 3). Such both types are predominantly corresponded to porous structure materials or agglomerates of spheres in quite regular array. The resulting inflection sharpness at a high relative pressures (p/p_0) was obtained from capillary condensation, indicating the existence of larger macropores and/or mesopores (Sing et al. 1985); which is corresponded to narrow slit-like pores. In fact, such macropores and mesopores are suggested to be the empty voids generated by the close nanoparticles aggregation. The surface area values of TiO_2 NPs and TiO_2 NWs are estimated to be 40.22 and 14.35 $m^2\ g^{-1}$, respectively.

SEM of TiO_2 NWs image reveals the TiO_2 NWs morphology and exhibits both uniform diameters ~ 100 nm and variable lengths ~ 5–10 μm, implying in remarkably ratios of enormous aspect up to 100 (Fig. 4a). TiO_2 NWs have a 50–100 nm diameter and length of few μm. TEM images of TiO_2 NWs exhibit

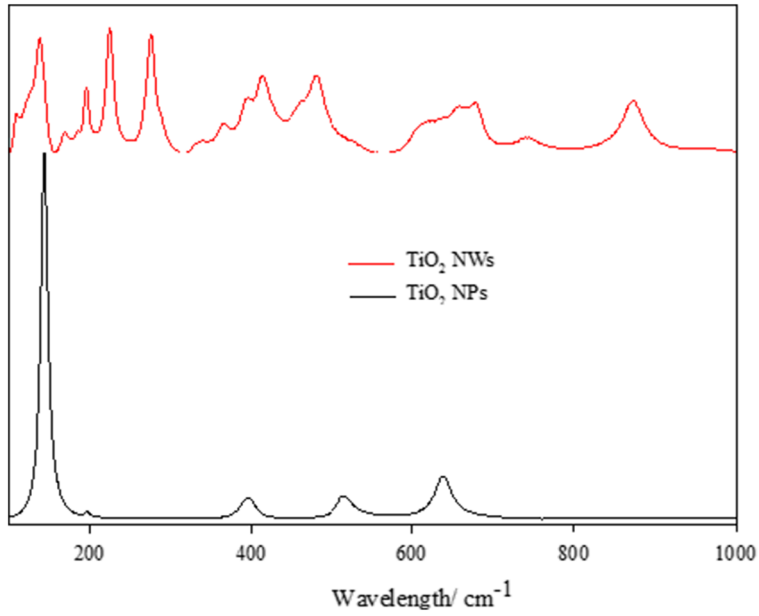

Fig. 2 Raman spectra for TiO_2 NPs calcined at 400 °C and TiO_2 NWs calcined at 800 °C

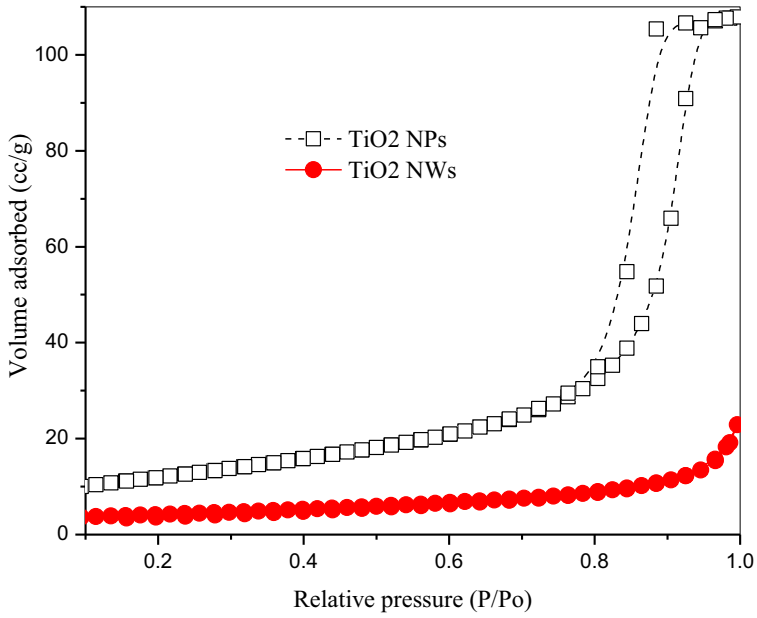

Fig. 3 The N_2 adsorption-desorption isotherms of TiO_2 NPs and TiO_2 NWs

obvious nanowire structures, and they have a 50–100 nm diameter and 2 μm length.

The diffuse reflectance spectra of TiO_2 NWs and TiO_2 NPs were displayed in Fig. 5a. The absorption edges of TiO_2 NPs were red-shifted to longer wavelength than TiO_2 NWs sample. The TiO_2 NPs and TiO_2 NWs onset absorbances were assigned at 374 nm and 315 nm, respectively. The band gap values were calculated for TiO_2 NWs and TiO_2 NPs via the Tauc equation as depicted in Fig. 5b. The relationship between $(F(R)E)^{1/2}$) and the harvested light energy (E) were employed to calculate the bandgap values as the following equation (Lei et al. 2014; Tang et al. 1994).

$$F(R)E^{1/2} = \left(\frac{(1-R)^2}{2R} \times h\upsilon\right)^{1/2}.$$

By intersecting the linear $(\alpha h\nu)^{1/2}$ curve part versus the photon energy axis ($h\nu$), the bandgap energy of TiO_2 NWs and TiO_2 NPs was estimated to be 3.36 and 3.08 eV respectively.

Results and discussions

Investigation of photocatalytic performance

Throughout the photocatalysis reactions, the photocatalytic degradation mechanism includes three steps involving of the resorcinol adsorption onto the surface of the photocatalyst, photocatalyst inducer by light absorption, and charge carrier transfer to generate active species and radical to degrade resorcinol molecules. The adsorption of resorcinol onto TiO_2 NWs or TiO_2 NPs surface was carried out in the dark for 60 min. The findings indicated that no resorcinol degradation was remarkably observed and also the photolysis of resorcinol without photocatalyst is insignificant. The TiO_2 NWs and TiO_2 photocatalysts were compared with commercial TiO_2-P25 by the calculation of the photodegradation rate derived by the photocatalytic degradation of resorcinol throughout UV illumination (Fig. 6). The prepared TiO_2 NWs and TiO_2 NPs exhibit similar photocatalytic efficiency, whereas the commercial TiO_2-P25 demonstrates lesser photocatalytic efficiency for resorcinol under the UV irradiation (Fig. 6a). TiO_2 NPs and TiO_2 NWs are capable of degrading about 98.7% and 98.4% of the initial resorcinol concentration as depicted in Fig. 6a, while the photocatalytic efficiency for the commercial TiO_2-P25 is about 83%. The photocatalytic degradation of resorcinol rate constants (k) over TiO_2 NPs and TiO_2 NWs is calculated and derived from Fig. 6b by the correlation between $\ln(C_t/C_o)$ and t (irradiation time), which is illustrated as the fundamental and functional photocatalytic performance of the TiO_2 NPs and TiO_2 NWs. The photodegradation of resorcinol is pursued the first-order kinetic model as follows: $-\ln(C_t/C_o) = kt$ where,

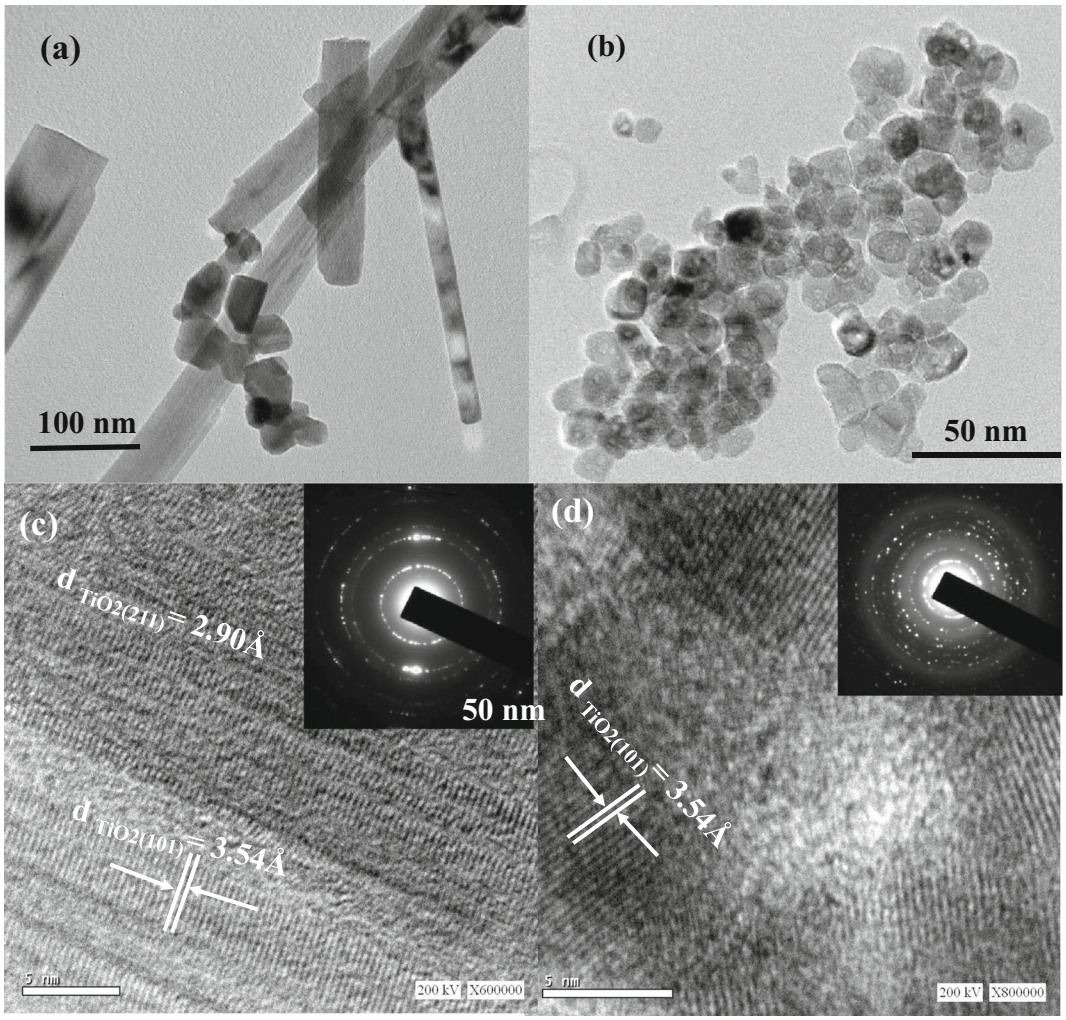

Fig. 4 **a** TEM image for TiO_2 NWs. **b** TEM image for TiO_2 NPs. **c** HR-TEM of TiO_2 NWs. **d** HR-TEM of the TiO_2 NPs. The corresponding SAED pattern of both TiO_2 NWs and TiO_2 NPs (inset, **c**, **d**) reveals the obtained brookite and anatase nanocrystalline

C_o and C_t are resorcinol concentrations (ppm) at time $t = 0$, and t (min), respectively, whereas k is the apparent rate constant (min^{-1}). The findings indicated that the k (min^{-1}) of TiO_2 NPs (0.0258 min^{-1}) and TiO_2 NWs (0.0254 min^{-1}) are more significant than that of commercial TiO_2-P25 (0.0078 min^{-1}) for 3.3 and 3.25 times, respectively. Photodegradation rates of resorcinol over TiO_2 NPs and TiO_2 NWs were estimated to be 12.24×10^{-7} mol L^{-1} min^{-1} and 10.79×10^{-7} mol L^{-1} min^{-1}, respectively, while the rate of commercial TiO_2-P25 is 5.77×10^{-7}mol L^{-1} min^{-1}. It was envisaged that the rate over TiO_2 NPs and TiO_2 NWs is higher two times than commercial TiO_2-P25. The difference between the photocatalytic activity of TiO_2 NWs, TiO_2 NPs, and commercial TiO_2-P25 cannot be attributed to various surface areas; owing to this is even more significant for the commercial P25 (Table 1). The photocatalytic degradation of resorcinol employing either TiO_2 NPs calcined at 400 °C or TiO_2 NWs calcined at 800 °C is comparable; although, the crystallinity, surface area, light absorption, and pores structure of TiO_2 NPs are higher than TiO_2 NWs. The TiO_2 NWs could demonstrate outstanding photocatalytic performance for the degradation of resorcinol due to they possess low charge carriers recombination rate and simple charge transit along the longitudinal dimension (Wu et al. 2012). Also, the high photocatalytic activity of TiO_2 NWs can be explained by the energy band and interface of brookite and anatase phases. On the other hand, TiO_2 NPs possess high photocatalytic efficiency due to they have mesoporous

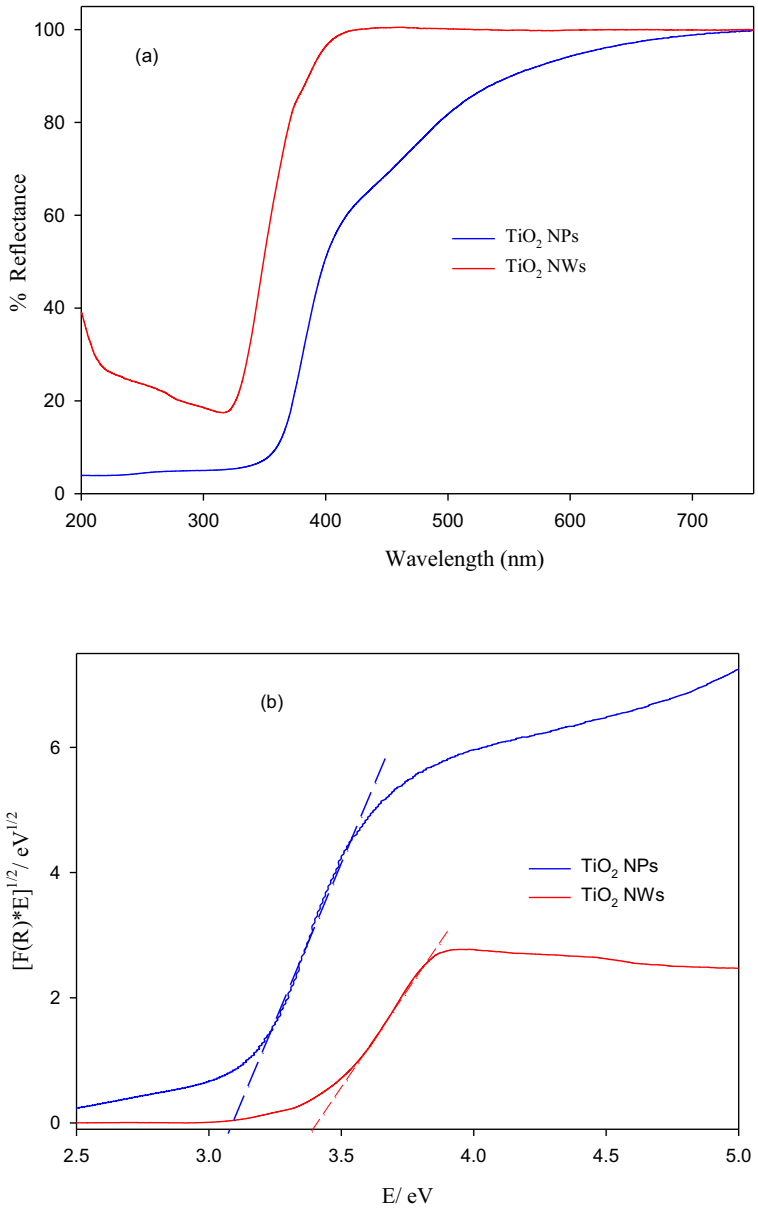

Fig. 5 **a** Diffuse reflectance spectra for TiO_2 NWs and TiO_2 NPs. **b** Plot of transferred Kubelka-Munk versus energy of the light absorbed of TiO_2 NWs and TiO_2 NPs.

structure materials, low bandgap, and high harvest light, high crystallinity, and small particle sizes. For saving energy, TiO_2 NPs calcined at 400 °C were chosen to be the optimum sample without loss of photocatalytic efficiency.

Photoluminescence (PL) is employed to determine the charge carrier efficiency. PL emission for both TiO_2 NWs and TiO_2 NPs was conducted with excitation at $\lambda = 320$ nm as depicted in Fig. 7. The blue sharp emission peak at 501 nm can be explained by the of charge carriers transition from Ti^{3+} to O_2 anion in a TiO_6^{2-} compound correlating with vacancies of O_2 (Al-Hajji et al. 2020). The intensity of TiO_2 NWs is higher than TiO_2 NPs. The reduction of intensity at TiO_2 NPs is related to the trap to trap electron transition to arrive at a recombination center. Therefore, we conclude that the photocatalytic degradation rate of TiO_2 NPs is slightly faster than TiO_2 NWs due to the slow recombination of photogenerated electrons and holes and decline the emission intensity.

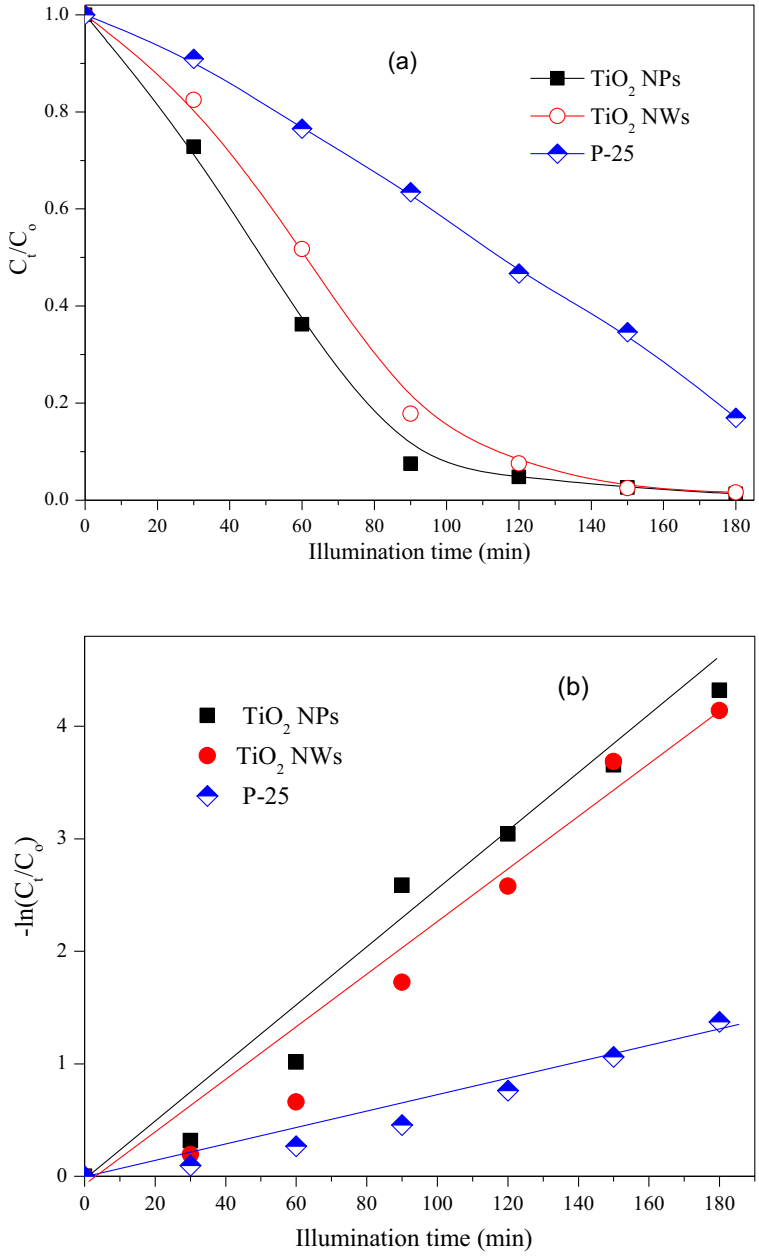

Fig. 6 Photocatalytic efficiencies of TiO_2 NWs and TiO_2 NPs compared with commercial TiO2-P25: Change in concentration vs. irradiation time in the presence of TiO_2 NWs **a** and TiO_2 NPs compared with commercial TiO2-P25 (**b**); ln (C/C_o) verses illumination time of TiO_2 NWs and TiO_2 NPs compared with commercial TiO2-P25 under UV light (**c**)

Table 1 Textural properties of TiO_2 NWs and TiO_2 NPs and commercial TiO_2-P25 and their photocatalytic performances

Photo-catalyst	S_{BET}/ m^2 g^{-1}	Bandgap/eV	$C_{S\ TiO2}$	k, min^{-1}	$r \times 10^7$ (mol L^{-1} min^{-1})	PE, %
TiO_2 NPs	40.22	3.08	14.20	0.0258	12.24	98.70
TiO_2 NWs	14.60	3.38	43.21	0.0254	10.79	98.40
P25 TiO_2-	50.0	3.26	28.76	0.0078	5.77	83.03

S_{BET} surface area, $C_{S\ TiO2}$ average crystallite size of TiO_2, k rate constant, *PE* photocatalytic efficiency

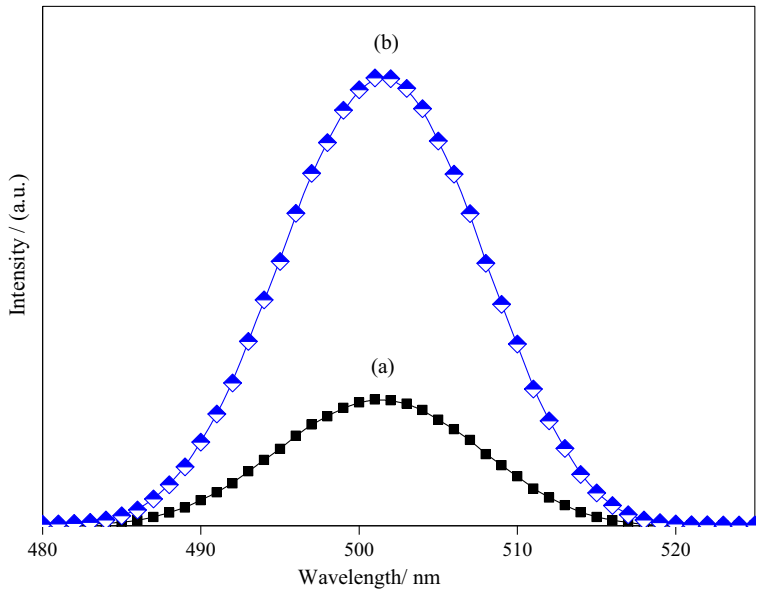

Fig. 7 Photoluminescence (PL) of TiO_2 NWs and TiO_2 NPs

Conclusions

In summary, the direct synthesis of TiO_2 NPs was prepared via a facile solvothermal, while TiO_2 NWs were prepared through a hydrothermal approach. The synthesized photocatalysts are capable of degrading about 98.7% and 98.4% of the initial resorcinol concentration, while the photocatalytic efficiency for the commercial TiO_2-P25 is about 83%. The photocatalytic degradation of resorcinol employing either TiO_2 NPs calcined at 400 °C or TiO_2 NWs calcined at 800 °C is comparable although the crystallinity, surface area, light absorption, and pores structure of TiO_2 NPs are more excellent than TiO_2 NWs. The rate constants (k) of TiO_2 NPs, TiO_2 NWs, and TiO_2-P25 were calculated to be 0.0258 min^{-1}, 0.0254 min^{-1}, and 0.0078 min^{-1}, respectively. The apparent rate constant k (min^{-1}) value of TiO_2 NPs and TiO_2 NWs is higher than that of commercial TiO_2-P25 for 3.3 and 3.25 times, respectively. For saving energy, TiO_2 NPs calcined at 400 °C are chosen to be the optimum sample without the loss of photocatalytic efficiency.

Acknowledgments Kuwait Institute for Scientific Research (KISR) is gratefully acknowledged for the instrumental facilities. Authors acknowledges the Kuwait University Research Administration support through RSPU facilities No. (GS 01/01, GS 01/05) and the Nanoscopy Science Center for carrying the TEM analysis.

Funding information The financial support received by the Kuwait Foundation for the Advancement of Sciences (KFAS) related to the Project EA071C under a contract number: PR17-12SC-01.

Compliance with ethical standards

Conflict of interest The authors declare that they have no conflict of interest.

References

Al-Hajji LA, Ismail AA, Al-Hazza A, Ahmed SA, Alsaidi M, Almutawa F, Bumajdad A (2020) Impact of calcination of hydrothermally synthesized TiO_2 nanowires on their photocatalytic efficiency. J Mol Struct 1200:127153

Brouwers MM, Besselink H, Bretveld RW, Anzion R, Scheepers PT, Brouwer A, Roeleveld N (2011) Estrogenic and androgenic activities in total plasma measured with reporter-gene bioassays: relevant exposure measures for endocrine disruptors in epidemiologic studies? Environ Int 37:557–564

Burda C, Chen XB, Narayanan R, El-Sayed MA (2005) Chemistry and properties of nanocrystals of different shapes. Chem Rev 105:1025

Chen X, Mao SS (2007) Titanium dioxide nanomaterials: synthesis, properties, modifications, and applications. Chem Rev 107:2891

Chen JS, Tan YL, Li CM, Cheah YL, Luan DY, Madhavi S, Boey FYC, Archer LA, Lou XW (2010) Constructing hierarchical spheres from large ultrathin anatase TiO_2 nanosheets with

nearly 100% exposed (001) facets for fast reversible lithium storage. J Am Chem Soc 132:6124

Deng D, Kim MG, Lee JY, Cho J (2009) Green energy storage materials: nanostructured TiO_2 and Sn-based anodes for lithium-ion batteries. Energy Environ Sci 2:818

Ding R, Wang K, Hong K, Zhang Y, Cui Y (2019) Hierarchical core-shell tungsten oxide/TiO_2 nanowires as an effective photocatalyst. Chem Phys Lett 714:156–159

Elsellami L, Dappozze F, Fessi N, Houas A, Guillard C (2018) Highly photocatalytic activity of nanocrystalline TiO_2 (anatase, rutile) powders prepared from $TiCl_4$ by sol-gel method in aqueous solutions. Process Saf Environ Prot 113:109–121

Hu W, Tong W, Li L, Zheng J, Li G (2011) Cation nonstoichiometry in multi-component oxidenanoparticles by solution chemistry: a case study on $CaWO_4$ for tailored structural properties. Phys Chem Chem Phys 13:11634–11643

Huang WB, Chen CY (2010) Photocatalytic degradation of diethyl phthalate (DEP) in water using TiO_2. Water Air Soil Pollut 207:349–355

Khedr TM, El-Sheikh SM, Ismail AA, Bahnemann DW (2019) Highly efficient solar light-assisted TiO_2 nanocrystalline for degradation of ibuprofen drug. Opt Mater 88:117–127

Law M, Greene LE, Johnson JC, Saykally R, Yang PD (2005) Nanowire dye-sensitized solar cells. Nat Mater 4:455

Lee H-G, Sai-Anand G, Komathi S, Gopalana A-I, Kang S-W, Lee K-P (2015) Efficient visible-light-driven photocatalytic degradation of nitrophenol by using graphene-encapsulated TiO_2 nanowires. J Hazard Mater 283:400–409

Lei XF, Xue XX, Yang H (2014) Preparation and characterization of Ag-doped TiO_2 nanomaterials and their photocatalytic reduction of Cr(VI) under visible light. Appl Surf Sci 321: 396–403

Li W, Zeng T (2011) Preparation of TiO_2 anatase nanocrystals by $TiCl_4$ hydrolysis with additive H_2SO_4. PLoS One 6:21082

Li Z, Cong S, Xu Y (2014) Brookite vs Anatase TiO_2 in the photocatalytic activity for organic degradation in water. ACS Catal 4:3273–3280

Liu C, Zhang L, Liu R, Gao Z, Yang X, Tu Z, Yang F, Ye Z, Cui L, Xu C, Li Y (2016) Hydrothermal synthesis of N-doped TiO_2 nanowires and N-doped graphene heterostructures with enhanced photocatalytic properties. J Alloys Compd 656:24–32

Mohamed RM, Ismail AA, Kadi MW, Bahnemann DW (2018) A comparative study on mesoporous and commercial TiO_2 photocatalysts for photodegradation of organic pollutants. J Photochem Photobiol A Chem 367:66–73

Pan ZW, Dai ZR, Wang ZL (2001) Nanobelts of semiconducting oxides. Science 291:1947

Pan J, Liu G, Lu GQ, Cheng H-M (2011) On the true photoreactivity order of {001}, {010}, and {101} facets of anatase TiO_2 crystals. Angew Chem Int Ed 50:2133

Qiu B, Xing M, Zhang J (2014) Mesoporous TiO_2 nanocrystals grown in situ on graphene aerogels for high photocatalysis and lithium-ion batteries. J Am Chem Soc 136:5852–5855

Sang Y, Zhao Z, Tian J, Hao P, Jiang H, Liu H, Claverie JP (2014) Enhanced photocatalytic property of reduced graphene oxide/TiO_2 nanobelt surface heterostructures constructed by an in situ photochemical reduction method. Small 10:3775–3782

Sing KSW, Everett DH, Haul RAW et al (1985) Reporting physisorption data for gas/solid systems with special reference to the determination of surface area and porosity. Pure Appl Chem 57:603–619

Sun CH, Yang XH, Chen JS, Li Z, Lou XW, Li C, Smith SC, Lu GQ, Yang HG (2010) Higher charge/discharge rates of lithium-ions across engineered TiO_2 surfaces leads to enhanced battery performance. Chem Commun 46:6129

Tang H, Prasad K, Sanilines R, Schmid PE, Levy F (1994) Electrical and optical properties of TiO_2 anatase thin films. J Appl Phys 75:2042–2047

Varghese OK, Paulose M, LaTempa TJ, Grimes CA (2009) High-rate solar photocatalytic conversion of CO_2 and water vapor to hydrocarbon fuels. Nano Lett 9:731–737

Wang X, Zhuang J, Peng Q, Li YD (2005) A general strategy for nanocrystal synthesis. Nature 437:121–124

Wu HB, Hng HH, Lou XW (2012) Direct synthesis of anatase TiO_2 nanowires with enhanced photocatalytic activity. Adv Mater 24:2567–2571

Xia YN, Yang PD, Sun YG, Wu YY, Mayers B, Gates B, Yin YD, Kim F, Yan YQ (2003) One-dimensional nanostructures: synthesis, characterization, and applications. Adv Mater 15: 353

Xia Y, Xiong YJ, Lim B, Skrabalak SE (2009) Shape-controlled synthesis of metal nanocrystals: simple chemistry meets complex physics? Angew Chem Int Ed 48:60

Yang J, Zhang X, Li B, Liu H, Sun P, Wang C, Wang L, Liu Y (2014) Photocatalytic activities of heterostructured TiO_2-graphene porous microspheres prepared by ultrasonic spray pyrolysis. J. Alloys Compd 584:180–184

Yu J, Wang Y, Xiao W (2013) Enhanced photoelectrocatalytic performance of SnO_2/TiO_2rutile composite films. J Mater Chem A 1:10727–10735

Zhang X, Pan JH, Du AJ, Fu W, Sun DD, Leckie JO (2009) Combination of one-dimensional TiO_2 nanowire photocatalytic oxidation with microfiltration for water treatment. Water Res 43:1179–1186

Zhu L, Gu L, Cao S, Cao X (2011) Direct production of a free-standing titanate and titania nanofiber membrane with selective permeability and cleaning performance. J Mater Chem 21:12503–12510